

**Brownian motors in variable-shape medium: Overdamped versus underdamped cases**M. F. Kepnang Pebeu,<sup>1,\*</sup> R. L. Woulaché,<sup>1,2</sup> and T. C. Kofane<sup>1,2</sup><sup>1</sup>Laboratory of Mechanics, Department of Physics, Faculty of Science, University of Yaounde I, P. O. Box 812, Yaounde, Cameroon<sup>2</sup>Centre d'Excellence Africain en Technologies de l'Information et de la Communication, University of Yaounde I, Cameroon (Received 24 April 2018; revised manuscript received 12 September 2018; published 7 November 2018)

In this paper, we investigate the statistical behavior of Brownian particles in a deformable traveling-wave potential in the absence of external load. We model the deformation of the system by the modified Remoissenet-Peyrard on-site potential, which is distinguished by its sine-Gordon shape. We examine numerically the effect of the deformed on-site potential with traveling speeds on the transport properties in overdamped as well as underdamped Brownian particles. Using the Langevin Monte Carlo method, we show that the average velocity of Brownian particles is an increasing function of the shape parameter in the overdamped case, and a decreasing function of the shape parameter in the underdamped case. It is found that, in the overdamped case, the numerical behavior of the average velocity of Brownian particles validates its analytical results. In the presence of the deformable traveling-wave potential, for negative as well as positive values of the shape parameter, the underdamped case favors the transport properties in the medium. The average velocity needed to cross the potential barriers is lowest in the underdamped case. Moreover, the effective diffusion coefficient in both cases exhibits peaks, and the diffusion process enhancement is discussed for some values of the shape parameter. Finally, in the underdamped case, by using the Smoluchowski equation and the finite-element methods, we analyze the distribution of Brownian particles in the deformed system.

DOI: [10.1103/PhysRevE.98.052107](https://doi.org/10.1103/PhysRevE.98.052107)**I. INTRODUCTION**

Brownian particles in periodic structures have attracted the attention of many researchers due to their multidisciplinary applications [1–10]. For instance, in biology, overdamped Brownian particles are molecular motors moving along a periodic structure performing basic tasks in living organisms, and they do not necessarily need an external applied load to accomplish their task, that is, carrying a load across a viscous environment [11,12]. Importantly, with modern microscopic techniques, superresolution has led to the discovery of a multitude of anomalous diffusion processes in living cells and complex fluids [13–16].

Likewise, Brownian particles have also been studied in detail in connection with superionic conductors, Josephson junctions, the dynamics of phase-locked loops [3,17–21], to mention but a few. The common feature of these latter cases is that they consist of species of high mobile particles considered to be Brownian particles moving on a periodic structure with diffusion coefficients comparable to those found in liquids [22–24]. In either case, Brownian particles are nanomachines that operate far from thermal equilibrium, using the thermal energy imbalance to perform mechanical work so as to generate the directed transport, with noise playing an important role in the process [25,26]. Thus, the drift of particles is generated when conditions such as the presence of thermal noise, the anisotropy of the medium, and the time dependence

are supplied by external variations of the constraints on the system [27]. Moreover, the interactions of the Brownian particles with the surrounding bath may be considered statistically rather than treating each Brownian particle individually due to the fluctuating forces described only by their statistical properties [28].

Indeed, most of the studies in the field of Brownian particles are modeled by physical systems having a rigid-shape on-site substrate potential. However, these systems with periodic structure, although interesting, describe realistic systems only with certain approximations. To obtain a physically more realistic periodic substrate for Brownian particles, the effects of physical parameters such as temperature and pressure should be considered. Under such constraints, some physical systems may undergo changes such as shape distortion, variation of crystalline structures, or conformational changes. Hence, it appears necessary to take into account the deformable character of the medium in Brownian particles. Indeed, deformable models have been considered both from mathematical and physical points of view. From a mathematical point of view, the foundations of deformable models represent a confluence of geometry, physics, and approximation theory. Geometry serves to represent object shape, physics imposes constraints on how the shape may vary over space and time, and optimal approximation theory provides the formal underpinnings of mechanisms for fitting the models to measured data. From a physical point of view, deformable models are viewed as elastic bodies that respond naturally to applied forces and constraints [29,30]. In fact, the term “deformable models” stems primarily from the use of elasticity theory at the physical level, generally with a Lagrangian dynamics setting. Furthermore,

---

\* Author to whom all correspondence should be addressed: [kepemafa@gmail.com](mailto:kepemafa@gmail.com)

in an overdamped case, aiming at a more realistic description on the molecular level, some authors [9] have added an internal variable, which becomes necessary if the time required to achieve, for instance, a conformational change is not small compared with other time scales.

In the present work, we study the transport properties of Brownian particles in a deformable traveling-wave potential both in overdamped and underdamped limits. Note, however, that the traveling-wave potential has been introduced by Borromeo *et al.* [31] to study Brownian surfers. They have shown that the traveling wave has the capability of dragging Brownian particles along. Moreover, the traveling-wave potential has been used by Li *et al.* [32] to characterize the orientation of a molecular motor's internal electric dipole in order to describe the nature of the interaction between the motors and the filaments, as well as the interplay of the interaction and ATP hydrolysis, in order to understand the physical mechanism of molecular motors. However, some works have been done on the dynamics of Brownian particles using the variable shape potential [33,34]. For example, in the overdamped case an optimal transport may be obtained by changing the shape of the system [33]. Moreover, in the presence of the deformable traveling-wave potential, systems with sharp wells and broad barriers may favor the transport under the influence of an applied load [34].

Most of the above-mentioned works deal with overdamped deformable Brownian systems in which the inertial term due to the finite mass of the particles is neglected. To the best of our knowledge, underdamped Brownian particles in the presence of a traveling variable shape potential have yet to be investigated.

Therefore, underdamped Brownian particles in the deformable traveling potential could model driven laser plasma waves, known to accelerate classical charged particles trapped by perpendicular propagating electrostatic waves [35], and where the deformed on-site potential can represent a substrate that has abnormalities and defects. This deformable substrate potential could also model ionic solids, whose species, considered to be noninteracting Brownian particles, occupy vacant sites of the rigid framework diffusing through a lattice [2].

This paper examines the dynamic properties of free Brownian particles under the influence of the deformable traveling-wave potential in the overdamped and underdamped cases, using the Langevin Monte Carlo method [36,37]. Since the traveling-wave potential speed can induce a nonzero current in the absence of any external force, we subsequently analyze, in both cases, the effective diffusion coefficient of particles moving in a periodic deformable traveling-wave potential.

The paper is organized as follows. In Sec. II we introduce the global model of free Brownian particles moving in a deformable traveling-wave potential, and the quantities of interest, such as the average velocity, the effective diffusion coefficient, and the Monte Carlo error. Analytical results of the transport properties of the overdamped Brownian particles are presented in Sec. III A along with a validation of the method using direct numerical simulations. The transport properties of the underdamped Brownian particles based on the Fokker-Planck equation are addressed in Sec. III B. Finally, our results are summarized in Sec. IV.

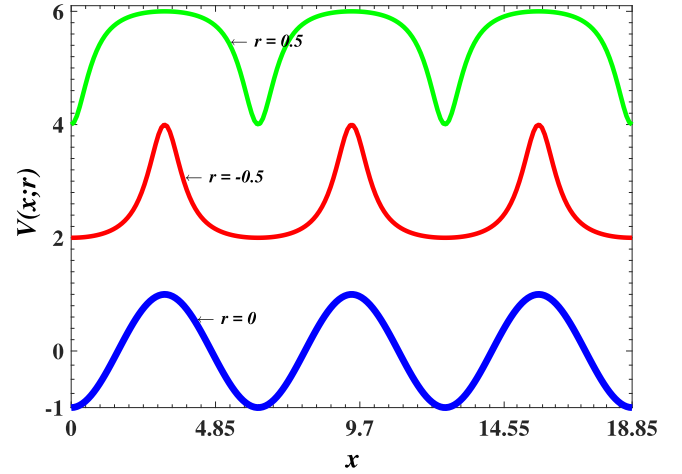


FIG. 1. Schematic representation of  $V(x; r)$  as a function of  $x$  for a few values of the shape parameter  $r$ , with  $\omega = 0$ .

## II. MODEL

We consider a Brownian particle of mass  $m$  free from any external load moving in a periodic traveling-wave potential with shape deformation. In this work, we choose the Remoissenet-Peyrard (RP) potential [38], modified according to [39]

$$V(x, t; r) = U \left[ \frac{(1+r)^2 [1 - \cos(x - \omega t)]}{(1-r)^2 + 2r[1 - \cos(x - \omega t)]} - 1 \right], \quad (1)$$

where  $|r| < 1$  represents the deformation parameter. We represent the RP potential for the traveling potential speed  $\omega = 0$  (see Fig. 1). The RP potential reduces to a sinusoidal shape for  $r = 0$ ; it provides broad wells separated by narrow barriers and deep narrow wells separated by broad flat barriers, respectively, for  $r < 0$  and  $r > 0$ , with  $U$  the potential height.

The dynamical behavior of the Brownian particles can be modeled by a stochastic differential equation of Langevin type written as [3]

$$m\ddot{x} + \gamma\dot{x} = -\frac{dV(x, t; r)}{dx} + \sqrt{2\gamma K_B T} \varepsilon(t), \quad (2)$$

which depicts the Markov process of Brownian particles. In Eq. (2), the overdot indicates differentiation with respect to time  $t$ .  $\gamma$  represents the friction coefficient of the medium,  $D = K_B T / \gamma$  is the diffusion coefficient of the Brownian particle,  $K_B$  is the Boltzmann constant, and  $T$  is the temperature of the bath. Assuming the environment to be an equilibrium heat bath with independent collisions,  $\varepsilon(t)$  is the Gaussian white noise of zero mean [ $\langle \varepsilon(t) \rangle = 0$ ], and it satisfies the fluctuation-dissipation relation  $\langle \varepsilon(t) \varepsilon(t') \rangle = 2D \delta(t - t')$ , where  $\delta(t)$  denotes the Dirac delta function, and  $t$  and  $t'$  are different times. The Dirac  $\delta$  function is a very convenient “function.” More exactly, it is the limiting case of a family of functions [40]. It has the property of singling out a particular value of a function  $f(t)$  at a value  $t = t_0$ . The function is characterized by the following properties:

$$\delta(t - t_0) = \begin{cases} 0 & \text{if } t \neq t_0, \\ \infty & \text{if } t = t_0, \end{cases}$$

in such a way that for any  $\epsilon > 0$ ,

$$\int_{t_0-\epsilon}^{t_0+\epsilon} \delta(t-t_0) dt = 1, \quad (3)$$

which means that the function  $\delta(t-t_0)$  has a very sharp peak at  $t = t_0$ , but the area under the peak is unity.

Since Eq. (2) is a stochastic differential equation, we consider a statistical ensemble of stochastic processes belonging to independent realizations of the random fluctuations  $\varepsilon(t)$ . The equivalent of the Langevin equation (2) is the Fokker-Planck or Smoluchowski equation for the distribution function  $P(x, v, t)$  in phase space  $(x, v)$ , written as

$$\frac{\partial}{\partial t} P(x, v, t) = L_F P(x, v, t), \quad (4)$$

with the Fokker-Planck operator  $L_F$ ,

$$L_F = -v \frac{\partial}{\partial x} + \left( \frac{\partial}{\partial v} \right) \left( \frac{\partial V(x, t; r)}{\partial x} + \gamma v \right) + D \frac{\partial^2}{\partial v^2}. \quad (5)$$

To understand the behavior of the Brownian particles in our system, we focus on the average velocity of Brownian particles. In fact, the average velocity of Brownian particles is perfectly sufficient to describe its dynamics in a system as well as its transport properties. In the overdamped case, an analytical expression of the average velocity for a Fokker-Planck equation was obtained earlier in previous works [34]. Here, we recall its expression (for more details of computation, see Ref. [34]),

$$\langle v \rangle = \omega + 2\pi C, \quad (6)$$

with

$$C = \frac{D[1 - \exp(\frac{2\pi\omega}{D})]}{\int_0^{2\pi} d\alpha \int_0^{2\pi} dx \exp(\frac{V(x+\alpha; r) - V(x; r) + \omega\alpha}{D})}. \quad (7)$$

Due to the nonlinearity of the RP potential, no analytical solution of Eq. (2) is available in the underdamped case. Thus, only its numerical solution is presented in this work. For the numerical treatment in both cases, we define the average velocity of Brownian particles in the long-time limit as

$$\langle v \rangle = \lim_{t \rightarrow \infty} \frac{\langle x(t) \rangle}{t}, \quad (8)$$

where  $\langle \dots \rangle$  means the ensemble average, which is the statistical average of the quantity inside the angular brackets at a given time over all systems of the ensemble. Other important quantities taken into account are the fluctuations around the average velocity of Brownian particles,  $V_{\text{av}} = \langle v^2 \rangle - \langle v \rangle^2$ , and the effective diffusion coefficient given by

$$D_{\text{eff}} = \lim_{t \rightarrow \infty} \frac{\langle x(t)^2 \rangle - \langle x(t) \rangle^2}{2t}, \quad (9)$$

while the Monte Carlo error is

$$\sigma = \frac{1}{\sqrt{L}} \sqrt{\langle v^2 \rangle - \langle v \rangle^2}, \quad (10)$$

with  $L$  the number of realizations of the fluctuating forces. The Brownian particles thus move with a velocity in the

range  $\langle v \rangle \equiv [\langle v \rangle - \sigma, \langle v \rangle + \sigma]$ . As previously mentioned by Machura *et al.* [41], if  $\sigma$  is greater than  $\langle v \rangle$ , the Brownian particles may move in the opposite direction, making the displacement of the particles less effective and complex.

### III. NUMERICAL RESULTS AND DISCUSSION

Focusing on the transport properties of the deformable system, the long-time limit of statistical quantities of interest is determined in terms of the statistical average over different realizations of the process in Eq. (2). We perform our numerical studies with the Euler algorithm. The time step is  $h = 10^{-2}$ . For initial conditions,  $x = 0$  at  $t = 0$ , the Brownian particle is at rest at the bottom of the deformable traveling-wave potential ( $\dot{x} = 0$ ). All quantities are averaged over 500–1000 different realizations, each of which evolves over  $t_{\text{max}} = 10^3$  for an overdamped case and  $t_{\text{max}} = 10^4$  for an underdamped case.

#### A. Overdamped Brownian motion

##### 1. The average velocity in the overdamped Brownian motion

We represent first the average velocity of the Brownian particles as a function of the traveling speed obtained through a numerical integration of Eq. (2), and second some analytical results [see Eq. (6)] for  $r = -0.5, 0.0$ , and  $0.5$  (see Fig. 2). In fact, the average velocity increases approximatively from 3% to 86% when  $r$  increases from 0 to  $\pm 0.5$  [34]. We note that our numerical solution is in good agreement with the analytic solution. However, this behavior requires a comment. Indeed, referring to Fig. 2, which depicts the average velocity of the Brownian particle as a function of the traveling-wave potential speed  $\omega$ , there exists a slight discrepancy with Fig. 2 of [34]. Moreover, as illustrated in these numerical simulations, the deformed system dissipated less thermal energy than the nondeformed system. In Ref. [34], the maximum average

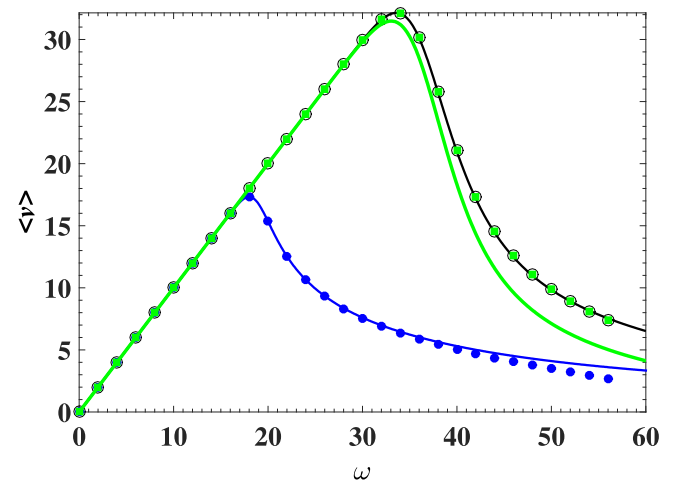


FIG. 2. Numerical solution of the average velocity obtained from Eq. (2) as a function of the traveling speed  $\omega$  for  $r = -0.5$  (black line),  $r = 0$  (blue line), and  $r = 0.5$  (green line). Also represented is its analytical solution [Eq. (5)] for  $r = -0.5$  (black open circle),  $r = 0$  (blue closed circle), and  $r = 0.5$  (green square). Other parameters used are  $U = 20$ ,  $\gamma = 1$ , and  $D = 0.5$ .

velocity of Brownian particles obtained from numerical simulation was greater for  $r = 0.5$  than that of  $r = -0.5$ , given by 18.7910 and 19.9589, respectively, whereas in Fig. 2, by using Eq. (8), the average velocities are greater for the shape parameter  $r = -0.5$  than  $r = 0.5$ , which are given by 32.1434 and 31.4817, respectively. Consequently, this last case exhibits a good enough agreement with the analytical result that we have derived [see Eq. (6)] [34]. In fact, in [34] the Kasdin algorithm was used to numerically simulate the stochastic differential equation, and then the formula

$$\langle v \rangle = \frac{1}{L} \sum_{i=1}^L \frac{1}{t_{\max}} \int_0^{t_{\max}} v(t) dt \quad (11)$$

was used to compute the average velocity of Brownian particles. Thus, in this context, it turns out that the use of Eq. (8) seems to be more reliable to address the stochastic differential equation since it matches well effectively with the theory proposed in [34]. Nevertheless, from a phenomenological point of view, the average velocity of Brownian particles in both cases presents the same shape. However, by varying the shape parameter with both formulas, some discrepancies related to numerical methods take place. This suggests that Eq. (11) is more appropriate when the system is subjected to an external periodic excitation [41–43], while Eq. (8) is more appropriate for systems that are not externally perturbed by a periodic excitation [21,44].

To understand the displacement of the Brownian particles in the traveling deformable system, we compute Eq. (10) together with Eq. (2) using the numerical method outlined above. It turns out that the Monte Carlo error  $\sigma$  as a function of the driving speed presents the same evolution as the average velocity for each value of the shape parameter. These fluctuations are always smaller than the corresponding average velocity (see Fig. 3). Also presented is the average velocity of Brownian particles given by Eq. (8) as a function of  $r$  (Fig. 4). The general behavior of  $\langle v \rangle$  is almost the same when the absolute value of  $r$  increases for a fixed value of

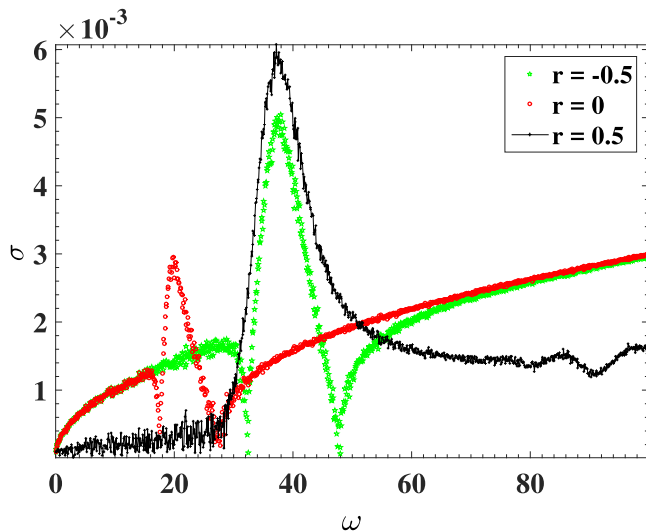


FIG. 3. Monte Carlo error  $\sigma$  vs  $\omega$  for different values of the shape parameter  $r$ , with  $U = 20.0$ ,  $D = 0.5$ , and  $\gamma = 1$ . Note that  $\sigma$  follows the same shape as the average velocity when  $|r|$  increases.

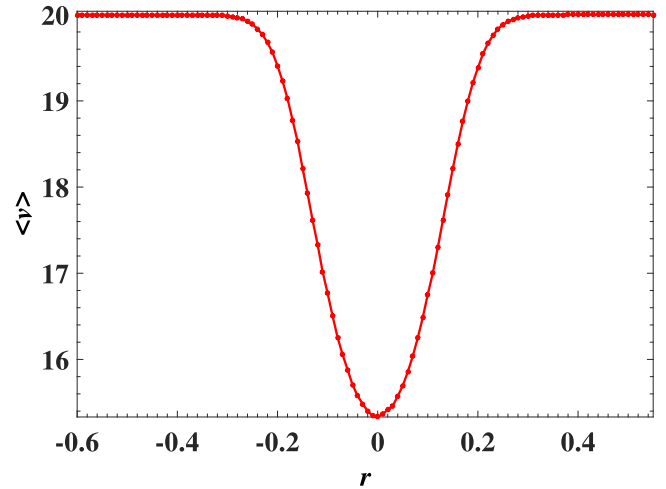


FIG. 4. Schematic representation of the average velocity of the Brownian particle in the overdamped case as a function of  $r$  for  $U = 20.0$ ,  $D = 0.5$ , and  $\omega = 20.0$ . This curve has nearly symmetric variations as the shape parameter evolves.

the traveling speed. Although the effect of each collision between the particle and its surrounding is important in the overdamped regime, the Monte Carlo errors prove that the transport properties of Brownian particles are performed with less turn-back. In the deformed system, and in the overdamped regime, the transport properties of Brownian particles are shown in the directed direction. Moreover, thermal energy is less dissipated in the deformable potential compared to the sinusoidal shape ( $r = 0$ ).

## 2. Diffusion in the overdamped Brownian motion

The behavior of the effective diffusion coefficient of the Brownian particle  $D_{\text{eff}}$  as a function of the traveling speed of the deformable potential for different values of the shape parameter  $r$  is investigated in the overdamped case. It exhibits a pronounced “resonance” peak at  $\omega = \omega_{\text{opt}}$  for different values of the shape parameter  $r$  (see Fig. 5). In fact, the presence of thermal fluctuations and/or the difference between the traveling speed of the potential and the velocity of the

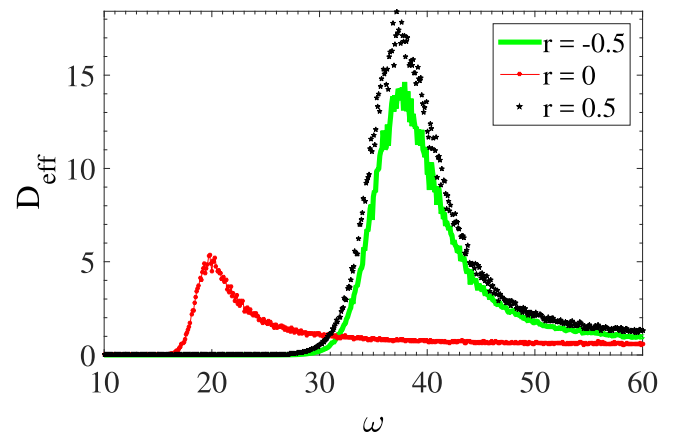


FIG. 5. Schematic representation of the effective diffusion of the Brownian particle in the overdamped regime as a function of the traveling speed  $\omega$  for a few values of  $r$ . The other parameters are  $U = 20$ ,  $D = 0.5$ , and  $\gamma = 1$ .

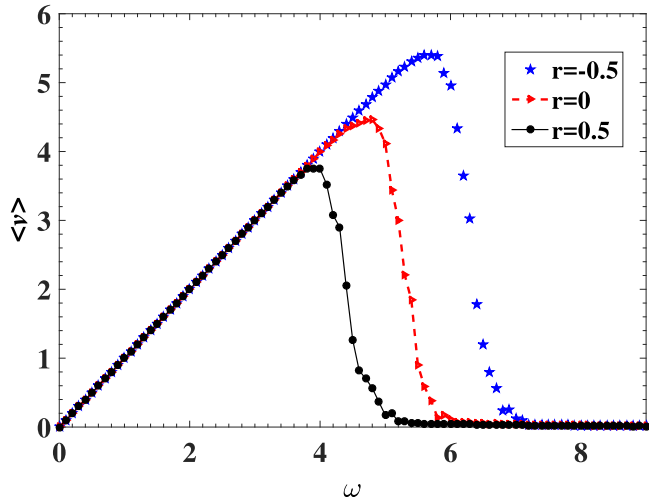


FIG. 6. Representation of the average velocity as a function of  $\omega$  for different values of the shape parameter  $r$  in the underdamped case. The transport properties are controlled by the shape parameter. The average velocity is higher for the negative value of the shape parameter,  $r = -0.5$ , than the positive values,  $r = 0$  and  $0.5$ . Note also that due to the presence of inertia, the potential energy is minimized. Other simulation parameters are  $K_B T = 0.56$ ,  $\gamma = 0.4$ , and  $m = 1$ .

surrounding medium may induce the motion in the system, thus inducing the diffusion of a Brownian particle. The effective diffusion is closely linked to the geometry of the system since peaks change when the shape parameter varies from sinusoidal to nonsinusoidal (see Fig. 5). For example, the peak of the effective diffusion coefficient is approximately equal to 5, 14, and 18 times the Einstein diffusion ( $D = K_B T / \gamma$ ) for  $r = 0, -0.5$ , and  $0.5$ , respectively.

**B. Underdamped Brownian motion**

*1. The average velocity in the underdamped Brownian motion*

In this subsection, we use the same numerical method as in the previous section to study the case in which the term  $m\ddot{x}$  is not neglected. The results of numerical simulations of the average velocity of Brownian particles  $\langle v \rangle$  as a function of the traveling speed  $\omega$  of the deformable potential are plotted in Fig. 6, while the corresponding Monte Carlo error  $\sigma$  as a function of the traveling speed of the deformable potential  $\omega$  is plotted in Fig. 7.

It should be noted that in the underdamped case, the weight of the Brownian particle plays an important role in its displacement in the system. It contributes to reducing the height of the potential barrier, as well as the time of displacement of the Brownian particle in the system. We can say that the dynamical behavior of the system, which is more regular, is controlled by the shape parameter  $r$ , as can be seen in Fig. 6. What is remarkable in this case is the behavior of Brownian particles whose average velocity decreases as the shape parameter  $r$  takes positive values. This behavior is contrary to what we observed in Fig. 2 in the case of overdamped Brownian motion. In fact, we notice that in the overdamped case, more energy is needed for the Brownian particle to cross the potential barrier. Thus, in the overdamped

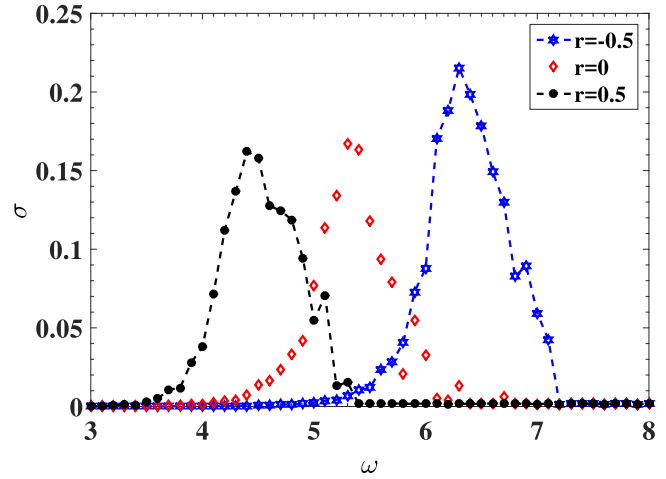


FIG. 7. Monte Carlo error representation in the underdamped case. Others simulation parameters are  $\gamma = 0.4$ ,  $K_B T = 0.56$ , and  $m = 1$ .

and underdamped Brownian motions, this crossover energy depends strongly on the shape parameter  $r$ . Once the particle crosses the potential barrier, there is a smooth decreasing of the energy provided by the potential as  $\omega$  increases and the Brownian particle slowly moves to a stable position where it oscillates. This behavior is illustrated by the smooth decrease seen in Fig. 2. Meanwhile, in the underdamped case the influence of both inertia and damping contributes to lower the potential barrier, so that when the particle crosses the barrier, it jumps quickly to the equilibrium position (see Fig. 6). The Monte Carlo error plotted in Fig. 7 follows the same behavior as  $\langle v \rangle$ , but it always remains lower. Thus, in both cases (overdamped and underdamped), the Brownian particle moves in the directed direction.

To gain good insight into the motion of the Brownian particle in the deformed traveling-wave potential in the underdamped case, we have plotted in Fig. 8 the maximum average

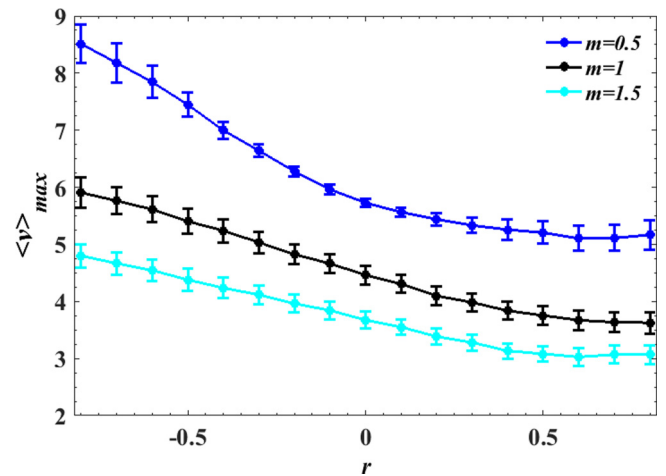


FIG. 8. Schematic representation of the maximum average velocity of the Brownian particle as a function of the shape parameter  $r$  in the underdamped case. Note here that, contrary to the overdamped case, the average velocity decreases as the shape parameter  $r$  evolves from negative values to positive ones.

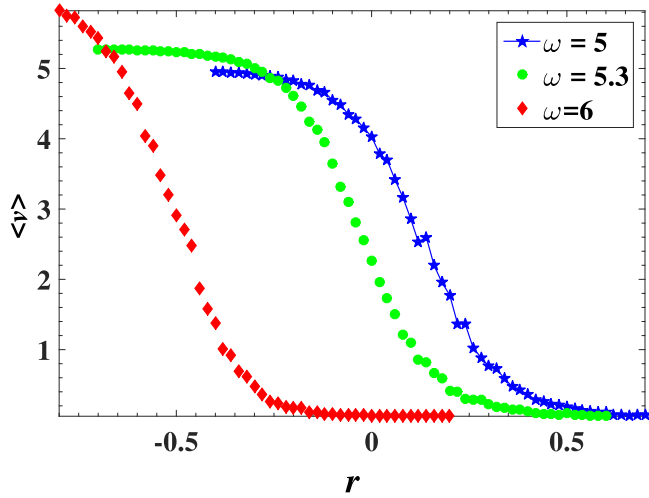


FIG. 9. Numerical simulation of the average velocity as a function of the shape parameter  $r$  for different values of  $\omega$ . We can see the decrease of the average velocity as the shape parameter  $r$  evolves from negative values to positive values for three values of the traveling potential speed. We also remark that the form of these curves follows the same shape as that of Fig. 8. This decrease comes from the fact that the necessary thermal energy for the particle to make a transition to the adjacent potential well is less dissipated in the deformable potential with broad wells and narrow deep wells, and the particle in this case has the necessary momentum to cross the potential barrier. Other simulation parameters are  $K_B T = 0.56$ ,  $\gamma = 0.4$ , and  $m = 1$ .

velocity of the Brownian particle as a function of the shape parameter  $r$  for several values of  $m$ , and the evolution of the average velocity obtained by direct simulation of Eq. (2) for  $m = 1$  (Fig. 9). It is shown in Figs. 8 and 9 that the error bars are much pronounced in the underdamped case. However, in all cases the maximum of  $\langle v \rangle$  is a decreasing function of the shape parameter  $r$ . So, we observe that the

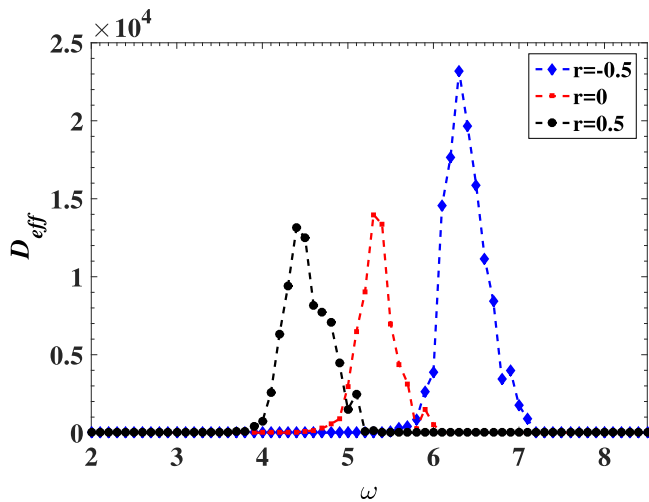


FIG. 10. Plot of the effective diffusion  $D_{\text{eff}}$  as a function of the traveling potential speed  $\omega$  for some values of the shape parameter  $r$  ( $r = -0.5, 0$ , and  $0.5$ ) as indicated in the figure. Other parameters of simulation are  $U = 5$ ,  $KT = 0.56$ ,  $\gamma = 0.4$ , and  $m = 1$ .

maximum average velocity of Brownian particles increases when the mass of the system decreases, thus evolving into the overdamped case, where the error bars are weak (see Fig. 8). This behavior of the average velocity may be due to the complex displacement of the Brownian particle in the system in the presence of inertia and thermal noise. These results are in good agreement with the theory of the chaotic behavior in the system when inertia is taken into account [45]. Moreover, we observe an abrupt decrease of the average velocity of the Brownian particles as a function of  $r$  compared to the overdamped case. One can say that the inertia has a positive influence on the transport properties of the system since it reduces the effect of fluctuations in the system and controls the transport properties.

This behavior of the Brownian particle in the underdamped case could be advantageous in the sense that even with lower energy, the unpinning of the system may be possible, but due to the inertia, the cargo may or may not reach the target.

## 2. Diffusion in the underdamped Brownian motion

In Fig. 10, we depict the effective diffusion as a function of the traveling-wave potential speed  $\omega$ , obtained numerically from Eqs. (2) and (9) for some values of the shape parameter  $r$ . Indeed, recent investigations have shown that under the effect of weak noise, and regardless of the value of the friction coefficient, there can appear a giant enhanced diffusion when the system undergoes an external constant load [1,21,46]. This is due to the presence of the locked-to-running transition that takes place when the Brownian particle diffuses on a one-dimensional periodic substrate and is subjected to a weak tilt. However, it has also been demonstrated through a Fokker-Planck equation that, in the absence of external constant load in the overdamped regime, a traveling-wave potential could induce a nonzero current  $\langle \dot{x}(t) \rangle \neq 0$  if the total energy of the Brownian particle is higher than that of the potential barrier [34]. Thus, when the particle drifts under the force exerted by the potential, the random switches between locked and running states also take place and cause an average spreading  $R(t) = \langle [x(t) - \langle x_{\text{CM}}(t) \rangle]^2 \rangle$  of particles around its average position. In our case (see Fig. 10 for  $m = 1$ ), this diffusion regime is very pronounced for negative values of the shape parameter  $r$ , and thus the optimum values of the traveling-wave potential speed that can be generated by the shape parameter  $r$  are also higher for the negative values of  $r$  (deep barriers and broad wells) than the positive ones. Moreover, for each peak corresponding to each value of the shape parameter  $r$ , there exists a value of  $\omega_{\text{opt}}$  for which the effective diffusion takes its maximum, which is slightly higher than that of the transition ( $\omega_{\text{opt}}$ , for average velocity). Indeed, for  $r = -0.5$ ,  $\omega_{\text{opt}} = 6.3$ ,  $D_{\text{eff,max}} = 2.3181 \times 10^4$ ; for  $r = 0$ ,  $\omega_{\text{opt}} = 5.3$ ,  $D_{\text{eff,max}} = 1.398 \times 10^4$ ; and finally for  $r = 0.5$ ,  $\omega_{\text{opt}} = 4.4$ ,  $D_{\text{eff,max}} = 1.3158 \times 10^4$ .

Next, we focus our attention on the effects of the shape parameter of the system on the peak values of the diffusion of Brownian particles in the underdamped case and the corresponding optimal deformable traveling-wave potential speed  $\omega_{\text{opt}}$  for several values of  $m$  ( $m = 0.5, 1, 1.5$ ). To achieve this purpose, Fig. 11 represents two plots. In the upper panel of this figure, the maximum value of the effective diffusion of

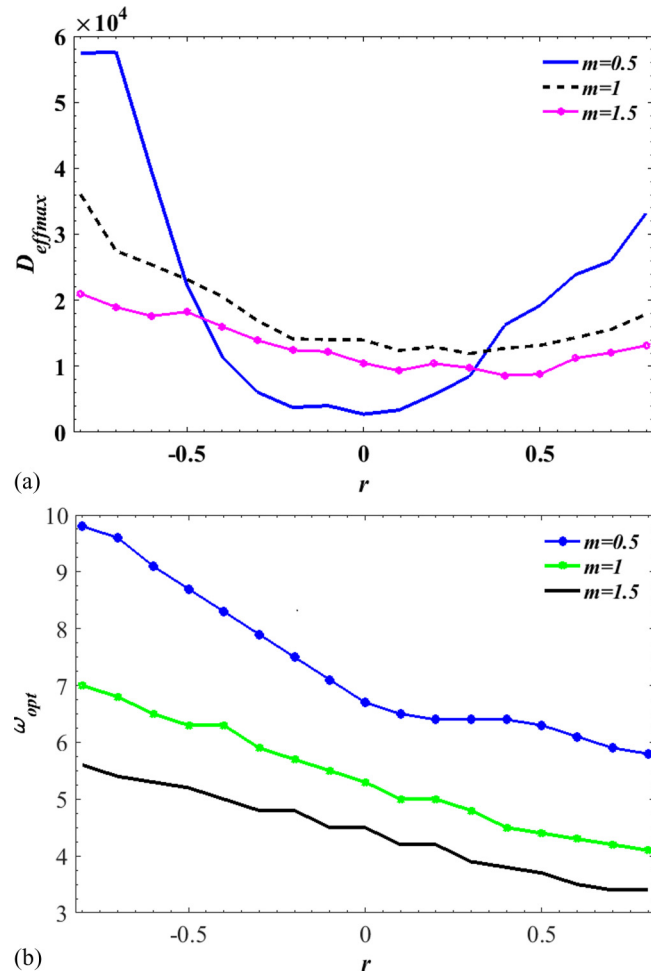


FIG. 11. Maximum values of the effective diffusion for  $m = 1$  of the Brownian particle and the corresponding traveling potential speed  $\omega_{opt}$  as a function of the shape parameter  $r$ .

the Brownian particle as a function of the shape parameter  $r$  is plotted for  $m = 0.5, 1, 1.5$ . In the lower panel, the corresponding deformable traveling-wave potential speed  $\omega_{opt}$  as a function of the shape parameter  $r$  is depicted for the same values of  $m$ . It can be seen in the upper panel of this figure that the maximum value of the effective diffusion is a decreasing function of the shape parameter  $r$  for  $m = 1$  and  $1.5$ . However, for  $m = 0.5$  one notes an almost parabolic behavior of the maximum diffusion. One should note that this case obviously gets closer to the overdamped case. In the lower panel, the corresponding traveling potential speed  $\omega_{opt}$  is also a decreasing function of the shape parameter  $r$  for all values of  $m$ . This behavior of the diffusion of the Brownian particle in the presence of the deformable traveling-wave potential may be due to the fact that, when the potential wells get narrow, the particle does not acquire the necessary space to cross the potential barrier, and then finds it difficult to disperse in the system, involving also the decrease of  $\omega_{opt}$  as the shape parameter evolves from negative to positive values. To completely illustrate the behavior of the effective diffusion in the deformable medium, we plot for  $m = 1$  the effective diffusion as a function of the shape parameter  $r$  for some values of the traveling-wave potential speed  $\omega = 5, 5.3, 6.3$  (Fig. 12). When  $\omega = 5$  the red curve presents a maximum at  $r = 0.2$ , for  $\omega = 5.3$  the blue curve presents a maximum at  $r = 0$ , while for  $\omega = 6.3$  the green curve shows a maximum at  $r = -0.5$ . As one might expect, the effective diffusion in this last case is very pronounced compare to the previous ones. This observation from numerical simulation corroborates effectively the previous observation, that is, in addition to the inertia term, the geometry of the potential, particularly the flat bottom, enhances the effective diffusion.

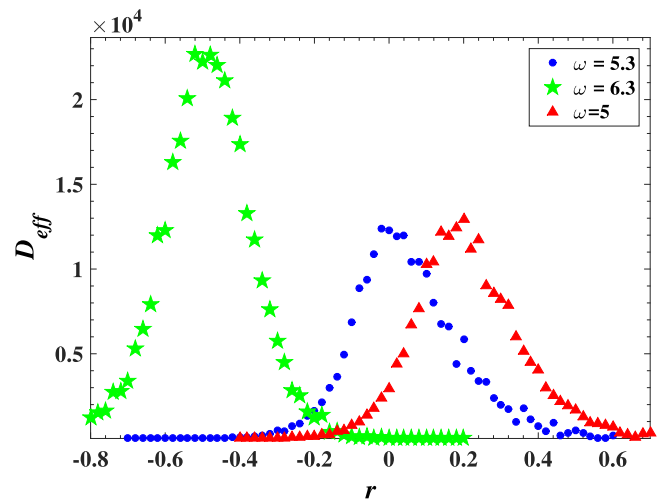


FIG. 12. Effective diffusion as a function of the shape parameter  $r$  for a particle moving in the deformable traveling potential for some values of potential speed  $\omega = 5, 5.3$ , and  $6$ , with the parameters previously used.

5.3, and 6.3 (Fig. 12). When  $\omega = 5$  the red curve presents a maximum at  $r = 0.2$ , for  $\omega = 5.3$  the blue curve presents a maximum at  $r = 0$ , while for  $\omega = 6.3$  the green curve shows a maximum at  $r = -0.5$ . As one might expect, the effective diffusion in this last case is very pronounced compare to the previous ones. This observation from numerical simulation corroborates effectively the previous observation, that is, in addition to the inertia term, the geometry of the potential, particularly the flat bottom, enhances the effective diffusion.

### 3. The Fokker-Planck treatment

In this subsection, an analysis of the distribution for various shape parameters  $r$  is presented. These distributions are

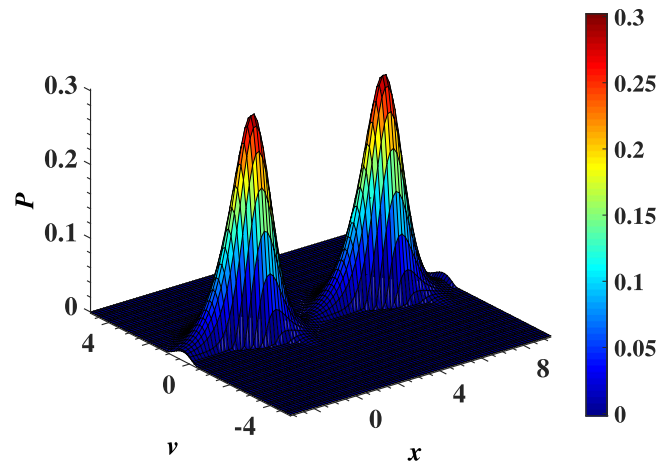


FIG. 13. Approximate solution of the Fokker-Planck equation showing the distribution of the Brownian particle in a deformable potential for  $r = 0$  at  $t = 1$ . This case reduces to the sine-Gordon case. The distribution exhibits two peaks corresponding to two adjacent minima of the potential.

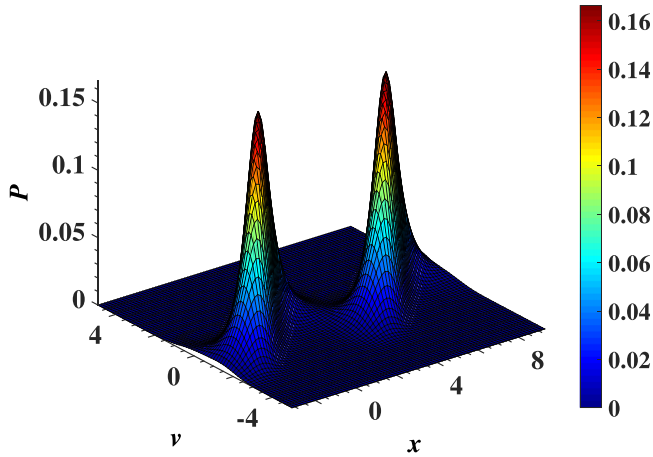


FIG. 14. Numerical simulation of the Fokker-Planck equation in a deformable potential for  $r = 0$ , obtained from the finite-element method at  $t = 1$ .

plotted for  $r = -0.5, 0$ , and  $0.5$  at  $t = 1, 2$  in the phase space  $(x, v)$  and also as the traveling potential speed is switched off ( $\omega = 0$ ). Thus, by using the semianalytic method developed in the Appendix as well as the numerical method (the finite-element method) for  $r = 0$ , we observe in Figs. 13 and 14 the presence of two narrow peaks corresponding to the minimum of the potential. For  $r = -0.5$ , we observe a large peak that also corresponds to the minimum of the potential (see Figs. 15 and 16). However, for  $r = 0.5$  we observe a splitting of the number of peaks. Let us recall here that the Fokker-Planck equation has been computed over two periods, characterized by the presence of two peaks, indeed, for  $r = -0.5$  the peaks are large compared to  $r = 0$  and  $0.5$ , respectively; this corresponds to a large dispersion of particles inside the potential well, indicating that the particles are spread out over a wider range of values due to the flat potential well and narrow barrier. However, for  $r = 0.5$ , which corresponds to a narrow well and a flat barrier, we observe a splitting of the number of peaks that pass from two peaks to four peaks (see

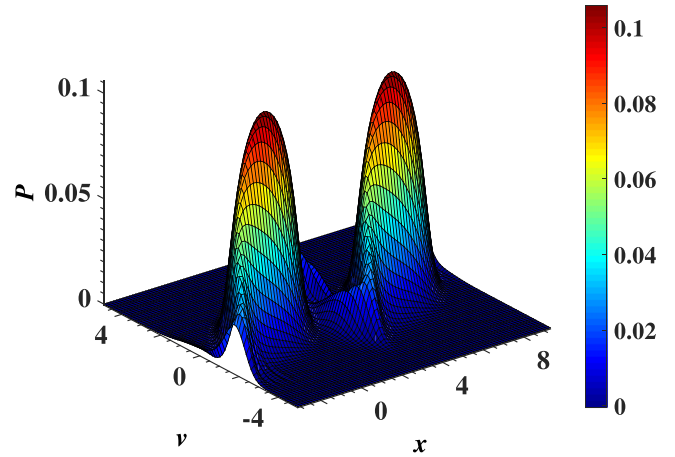


FIG. 16. Numerical simulation of the Fokker-Planck equation in a deformable potential for  $r = -0.5$ , obtained from the finite-element method at  $t = 2$ .

Figs. 17 and 18). A similar behavior is observed by adopting the semianalytic method, although the two other peaks are not well visible. To explain all these behaviors, let us analyze the different periods of oscillation of particles in different forms of potential. The period of oscillation around the ground states in the deformable potential is  $T_r = 2\pi/\omega_r$ , with  $\omega_r = V''(x_0)$  given by  $\omega_r = \frac{U(1+r)^2}{1+r^2}$ . Thus, the oscillation periods for  $r = -0.5, 0$ , and  $0.5$  are given by  $T_1 = 10\pi U$ ,  $T_2 = 2\pi U$ , and  $T_3 = 1.11\pi U$ , respectively. In fact, the time that the particles take in shrinking the potential well to perform oscillations is smaller with respect to  $r = 0$  and  $-0.5$ . For  $r = 0.5$ , as has been said before, the particles do not acquire the necessary momentum to cross the potential barrier to the adjacent well and consequently oscillate continuously around several equilibria positions due to the thermal energy, so that the metastable positions can take place leading to the appearance of new extrema (multimodality) in the probability distribution.

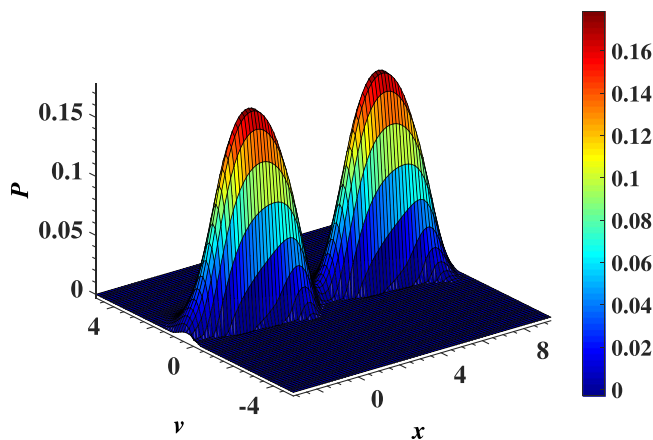


FIG. 15. Approximate solution of the Fokker-Planck equation giving the distribution of the Brownian particle in a deformable potential for  $r = -0.5$  at  $t = 2$ . This case also exhibits two modes corresponding to two adjacent minima of the potential.

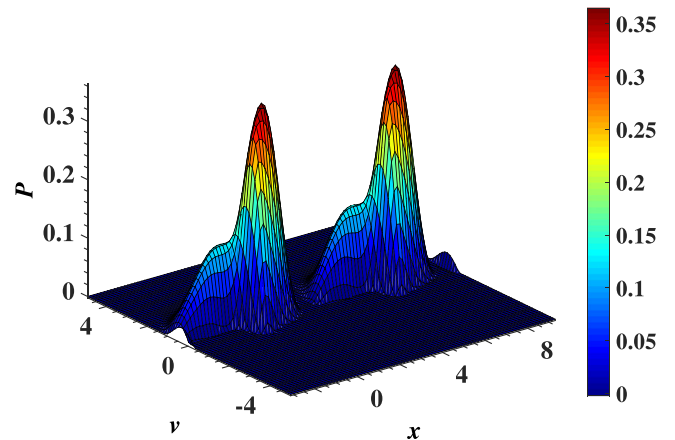


FIG. 17. Approximate solution of the Fokker-Planck equation showing the distribution of the Brownian particle in a deformable potential for  $r = 0.5$  at  $t = 2$ . This case tends to split in several modes.

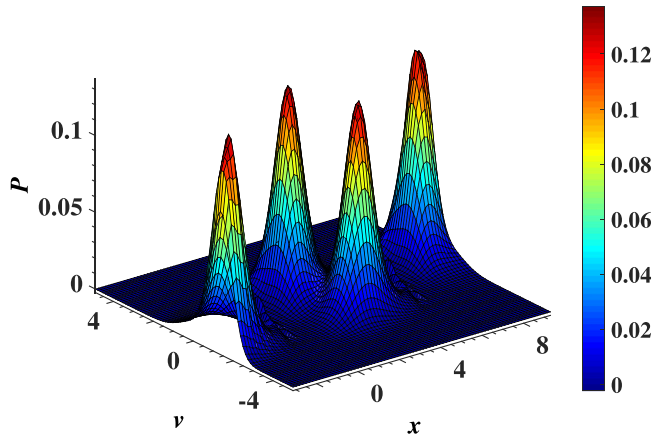


FIG. 18. Numerical simulation of the Fokker-Planck equation in a deformable potential for  $r = 0.5$  at  $t = 2$ , obtained from the finite-element method. We observe a complete splitting of modes that pass from two modes in the previous cases to four modes. This may be due to the metastable states that take place in the system, which is due to a deep-well potential and broad barriers.

**IV. CONCLUSION**

In this work, we have studied the behavior of Brownian particles in a deformable traveling medium, taking into account a white-noise source. Two aspects of the dynamics have been examined: the case without inertia (the overdamped case), and the case with inertia (the underdamped case). We have focused our attention on the statistical properties of Brownian particle motion (average velocity, Monte Carlo error bars, effective diffusion, and distribution) in the deformable traveling-wave medium. It was revealed that in the presence of the deformable traveling-wave potential, in the overdamped as well as underdamped Brownian motions, each maximum value of the average velocity of Brownian particles is a function of the shape parameter  $r$ . However, the effective diffusion in both cases (overdamped and underdamped cases) and the distribution of Brownian particles depend strongly on the shape parameter  $r$ . It is also shown that even in the presence of the deformable traveling-wave potential, the average velocity needed for the Brownian particle to cross the potential barrier, for each value of the shape parameter, is always smaller in the underdamped case. The Brownian particles are increasingly affected by inertia and also by damping. Comparing the behavior of the Brownian particle in both cases, the maximum average velocity values increase with the shape parameter  $r$  in the overdamped case, while in the underdamped case the transport properties are controlled by the shape parameter  $r$ , i.e., the average velocity of Brownian particles increases when the potential wells broaden. When the deformable traveling potential speed increases, the Brownian particle experiences significant reverse motion, and it is almost at rest very quickly compared with the overdamped case. A comparative analysis between the values of the maxima of the average velocity of Brownian particles and the direct numerical simulation of the nonlinear stochastic differential equation has shown that in the underdamped case, the average velocity of the particle depends on the deformable traveling potential speed  $\omega$ . Moreover, we

have observed that the interplay between the mass, the noise, and the force generated by the potential can lead to complex behavior of Brownian particles. Monte Carlo error bars have confirmed the directed motion of the Brownian particle in the overdamped and underdamped cases. It has also been shown that in the absence of any external load, the system in both the overdamped and underdamped cases undergoes an enhancement diffusion. Indeed, in both cases the effective diffusion is always greater than that of Einstein, regardless of the shape parameter  $r$ . Moreover, in the underdamped case we have observed a “giant” enhancement diffusion induced by the geometry of the system. Then, the particle diffuses more freely in the potential with  $r < 0$  compared with  $r > 0$ , due to the presence of the mass of the Brownian particle. However, in the overdamped case the effective diffusion exhibits a peak for different values of the shape parameter  $r$ , and these peaks are less pronounced compare with the underdamped case.

We have also shown numerically and by the semianalytical method, through the Fokker-Planck equation in the underdamped case, that the distribution can present several modes for positive values of the shape parameter. This comes from the fact that the metastable states can take place in the system, while for the negative value of the shape parameter and the sine-Gordon case ( $r = 0$ ), the birth of each mode obviously corresponds to a minimum of the potential, although for  $r < 0$  the distribution is very large.

**ACKNOWLEDGMENTS**

M.F.K. thanks the Stellenbosch University where a part of this work was carried out during his visit under the Fellowship “Pafroid” project funded by the European Commission, which is gratefully acknowledged. We are indebted to Hugo Touchette from Stellenbosch University for useful discussions and orientations. T.C.K. thanks the African University of Science and Technology–Abuja Nigeria (AUST) and the Nelson Mandela Institution (NMI) where a part of this work was carried out during his visit. Thanks to the Electronic Journal Delivery Service of the International Centre of Theoretical Physics (ICTP) for providing valuable references used in this study.

**APPENDIX: SEMIANALYTICAL TREATMENT OF THE FOKKER-PLANCK EQUATION**

In the case of  $r = 0$ , we have the particular case of the sine-Gordon potential, which leads to the sinusoidal case. Therefore, the analytical solution of the Fokker-Planck equation can be easily approximated by the matrix continued fraction (MCF) shown in Refs. [3,47,48] and more recently in [21]. Nevertheless, we are going to use the spectral method, or again a “semianalytical” method, to approximate the solution [49]. In fact, according to Refs. [3,21,48] we set

$$P(x, t, v) = \sum_{n=0}^{\infty} C_n(x, t) \psi_n(v), \tag{A1}$$

where  $C_n(x, t)$  are the expansion coefficients. As was mentioned before, the coupled system of  $C_n(x, t)$  may be solved using matrix continued fraction methods, notably for the cosine potential, parabolic, and so on. The  $\psi_n(v)$  is the

$n$ th-order Hermite polynomial, and its factorial factor is chosen so that the coefficient matrix of the induced partial differential equation system for  $C_n$  is symmetric, which implies that this partial differential equation is hyperbolic. The Hermite functions obey the following recurrence relations:

$$\frac{d\psi_n(v)}{dv} = -\alpha\sqrt{2(n+1)}\psi_{n+1}(v), \quad (\text{A2})$$

$$\frac{d^2\psi_n(v)}{dv^2} = -\alpha^2\sqrt{4(n+1)(n+2)}\psi_{n+2}(v), \quad (\text{A3})$$

$$v\frac{d\psi_n(v)}{dv} = \sqrt{(n+1)(n+2)}\psi_{n+2}(v) - (n+1)\psi_n(v) \quad (\text{A4})$$

$$v\psi_n(v) = \left(\frac{\alpha}{\sqrt{2}}\right)(\sqrt{n+1}\psi_{n+1}(v) + \sqrt{n}\psi_{n-1}(v)). \quad (\text{A5})$$

By inserting Eq. (A1) in the time-dependent Fokker-Planck equation, Eq. (4), and applying Eqs. (A2)–(A5), we obtain the following coupled system, which constitutes a partial differential equation system that obeys the expansion coefficients:

$$\begin{aligned} \frac{\partial C_n(x, t)}{\partial t} = & -\frac{\alpha\sqrt{n}}{\sqrt{2}}\frac{\partial C_{n-1}(x, t)}{\partial x} - \frac{\alpha\sqrt{n+1}}{\sqrt{2}}\frac{\partial C_{n+1}(x, t)}{\partial x} \\ & - \frac{\sqrt{2n}}{\alpha}[V'(x, t)]C_{n-1} - \gamma n C_n(x, t) \\ & + \sqrt{n(n-1)}\left(\frac{2\gamma KT}{\alpha^2} - \gamma\right)C_{n-2}(x, t). \end{aligned} \quad (\text{A6})$$

To solve Eq. (A6), we use the spectral method of order  $N$ . This method consists of solving the first  $(N+1)$  equation of (A6) for the  $N+1$  expansion coefficients  $C_0, C_1, C_2, \dots, C_N$ . Thus, all the functions  $C_n(x, t)$ ,  $n \geq N+1$ , are set to 0, i.e., take the approximate solution to  $P(x, v, t)$  as the following truncated series  $P_N(x, v, t)$ .

$\mathbf{C}$  denotes an  $(N+1)$ -dimensional column vector defined by  $\mathbf{C} = \mathbf{C}(\mathbf{x}, \mathbf{t}) = [C_0(x, t), C_1(x, t), \dots, C_N(x, t)]^T$ . The coupled system (A6) becomes

$$\frac{\partial \mathbf{C}}{\partial t} = -\alpha \mathbf{R} \frac{\partial \mathbf{C}}{\partial x} + \mathbf{S} \mathbf{C}, \quad (\text{A7})$$

where  $\mathbf{R}$  and  $\mathbf{S}$  are  $(N+1) \times (N+1)$  matrices given by

$$\mathbf{R} = \begin{pmatrix} 0 & \alpha_1 & & & \\ \alpha_1 & 0 & \alpha_2 & & \\ & \ddots & \ddots & \ddots & \\ & & & & \alpha_N \\ & & & & & \alpha_N \end{pmatrix} \quad (\text{A8})$$

and

$$\mathbf{S} = \begin{pmatrix} 0 & 0 & \cdots & 0 & \cdots \\ -\frac{\sqrt{2}}{\alpha}A & -\gamma & 0 & \cdots & \\ 0 & -\frac{2}{\alpha}A & -2\gamma & 0 & \cdots \\ 0 & 0 & -\frac{\sqrt{6}}{\alpha}A & -3\gamma & \cdots \\ \vdots & \ddots & \ddots & \ddots & \ddots \end{pmatrix} \quad (\text{A9})$$

with  $A = \frac{\partial V(x, t)}{\partial x}$  and  $\alpha_n = \sqrt{n/2}$ .  $\mathbf{R}$  is a symmetric matrix, so the set of its eigenvectors is also an orthogonal matrix; let us define the eigenvectors as  $U = [u_0, u_1, \dots, u_N]$ . It is easily verified that  $U^T R U = \Delta = \text{diag}[\lambda_0, \lambda_1, \lambda_2, \dots, \lambda_N]$ . If we multiply Eq. (A7) by  $U^T$ , we obtain

$$\frac{\partial \tilde{\mathbf{C}}}{\partial t} = -\alpha \Delta \frac{\partial \tilde{\mathbf{C}}}{\partial x} + \tilde{\mathbf{S}} \tilde{\mathbf{C}}, \quad (\text{A10})$$

with  $\tilde{\mathbf{C}} = U^T \mathbf{C}$  and  $\tilde{\mathbf{S}} = U^T \mathbf{S} U$ . Since Eq. (A10) is a nonlinear and coupled system, it is difficult to obtain an analytical solution for all the different modes; thus, the finite-difference method should be used to approximate the solution  $\tilde{\mathbf{C}}(x, t)$ . It is for this reason that we call it the “semianalytic method.” To ensure the stability of the finite-difference method in our case, the different schemes are used according to the sign of the eigenvalue of the matrix  $R$ . So, for  $\lambda_i < 0$ , the forward space difference scheme should be used, and for  $\lambda_i > 0$ , the backward space difference scheme should be used. Combining all this, we obtain the following different numerical schemes:

$$\begin{aligned} \tilde{C}_i(x, t + dt) = & \tilde{C}_i(x, t) - \frac{\alpha \lambda_i dt}{dx} [\tilde{C}_i(x, t) - \tilde{C}_i(x - dx, t)] \\ & + dt (\tilde{\mathbf{S}} \tilde{\mathbf{C}})_i(x, t) \end{aligned} \quad (\text{A11})$$

for  $\lambda_i > 0$ ,

$$\begin{aligned} \tilde{C}_i(x, t + dt) = & \tilde{C}_i(x, t) - \frac{\alpha \lambda_i dt}{dx} [\tilde{C}_i(x + dx, t) - \tilde{C}_i(x, t)] \\ & + dt (\tilde{\mathbf{S}} \tilde{\mathbf{C}})_i(x, t) \end{aligned} \quad (\text{A12})$$

for  $\lambda_i < 0$ , and

$$\tilde{C}_i(x, t + dt) = \tilde{C}_i(x, t) + dt (\tilde{\mathbf{S}} \tilde{\mathbf{C}})_i(x, t) \quad (\text{A13})$$

for  $\lambda_i = 0$ . So, the  $C_i(x, t)$  are substituted into Eq. (A1) to approximate the solution of the Fokker-Planck equation. To illustrate this, we chose  $N = 9$ , and some results displayed in the text show the different approximation forms.

- [1] P. Hänggi and F. Marchesoni, *Rev. Mod. Phys.* **81**, 387 (2009).
- [2] P. Hänggi, F. Marchesoni, and F. Nori, *Ann. Phys. (Leipzig)* **14**, 51 (2005).
- [3] H. Risken, *The Fokker-Planck Equation: Methods of Solution and Applications* (Springer, Berlin, 1984).
- [4] H. Touchette, T. Prellberg, and W. Just, *J. Phys. A* **45**, 395002 (2012).

- [5] H. Touchette, E. Van der Straeten, and W. Just, *J. Phys. A* **43**, 445002 (2010).
- [6] A. Gnoli, A. Puglisi, and H. Touchette, *Europhys. Lett.* **102**, 14002 (2013).
- [7] A. Baule, H. Touchette, and E. G. D. Cohen, *Nonlinearity* **24**, 351 (2011).
- [8] K. Svoboda, P. P. Mitra, and S. M. Block, *Proc. Natl. Acad. Sci. (U.S.A.)* **91**, 11782 (1994).

- [9] F. Jülicher, A. Ajdari, and J. Prost, *Rev. Mod. Phys.* **69**, 1269 (1997).
- [10] B. Louis, doctoral thesis, Université de la Sorbonne, France, 1900.
- [11] M. E. Fisher and A. B. Kolomeisky, *Proc. Natl. Acad. Sci. (U.S.A.)* **96**, 6597 (1999).
- [12] S. Leibler, *Nature (London)* **370**, 412 (1994).
- [13] R. Metzler, J.-H. Jeon, A. G. Cherstvy, and E. Barkai, *Phys. Chem. Chem. Phys.* **16**, 24128 (2014).
- [14] Y. Meroz and I. M. Sokolov, *Phys. Rep.* **573**, 1 (2015).
- [15] E. Barkai, Y. Garini, and R. Metzler, *Phys. Today* **65**(8), 29 (2012).
- [16] A. S. Bodrova, A. V. Chechkin, A. G. Cherstvy, H. Safdari, I. M. Sokolov, and R. Metzler, *Sci. Rep.* **6**, 30520 (2016).
- [17] B. Lindner and E. M. Nicola, *Eur. Phys. J. Spec. Top.* **157**, 43 (2008).
- [18] P. Reimann, C. Van den Broeck, H. Linke, P. Hänggi, J. M. Rubi, and A. Pérez-Madrid, *Phys. Rev. Lett.* **87**, 010602 (2001).
- [19] I. G. Marchenko, I. I. Marchenko, and V. I. Tkachenko, *JETP Lett.* **106**, 242 (2017).
- [20] Z.-W. Bai and W. Zhang, *Chem. Phys.* **500**, 62 (2018).
- [21] B. Lindner and I. M. Sokolov, *Phys. Rev. E* **93**, 042106 (2016).
- [22] A. Asaklil, M. Mazroui, and Y. Boughaled, *Eur. Phys. J. B* **10**, 91 (1999).
- [23] W. Dieterich, P. Fulde, and I. Peschel, *Adv. Phys.* **29**, 527 (1980).
- [24] W. Dieterich, *Solid State Ion.* **5**, 21 (1981).
- [25] M. Kostur, L. Machura, P. Hänggi, J. Luczka, and P. Talkner, *Physica A* **371**, 20 (2006).
- [26] A. Kenfack, J. Gong, and A. K. Pattanayak, *Phys. Rev. Lett.* **100**, 044104 (2008).
- [27] M. Borromeo and F. Marchesoni, *Chaos* **15**, 026110 (2005).
- [28] D. L. Ermak and H. Buckholz, *J. Comput. Phys.* **35**, 169 (1980).
- [29] R. Hegadi, A. Kop, and M. Hangarge, A Survey on Deformable Model and its Applications to Medical Imaging, Special Issue on RTIPPR (Recent Trends in Image Processing and Pattern Recognition (IJCA, 2010), pp. 64–75.
- [30] D. Terzopoulos and K. Fleischer, *Visual Comput.* **4**, 306 (1988).
- [31] M. Borromeo and F. Marchesoni, *Phys. Lett. A* **249**, 199 (1998).
- [32] Y.-X. Li, X.-Z. Wu, and Y.-Z. Zhuo, *Physica A* **286**, 147 (2000).
- [33] X. Q. Huang, P. Deng, J. W. Xiong, and B. Q. Ai, *Eur. Phys. J. B* **85**, 162 (2012).
- [34] R. L. Woulache, F. M. Kepnang Pebeu, and T. C. Kofane, *Physica A* **460**, 326 (2016).
- [35] T. Katsouleas and J. M. Dawson, *Phys. Rev. Lett.* **51**, 392 (1983).
- [36] P. R. Bevington and D. K. Robinson, *Data Reduction and Error Analysis for the Physical Sciences* (McGraw-Hill, New York, 2003).
- [37] N. Metropolis, A. W. Rosenbluth, M. N. Rosenbluth, A. H. Teller, and E. Teller, *J. Chem. Phys.* **21**, 1087 (1953).
- [38] M. Peyrard and M. Remoissenet, *Phys. Rev. B* **26**, 2886 (1982).
- [39] G. Costantini, F. Marchesoni, and M. Borromeo, *Phys. Rev. E* **65**, 051103 (2002).
- [40] F. Reif, *Fundamentals of Statistical and Thermal Physics* (McGraw-Hill, Singapore, 1985).
- [41] L. Machura, M. Kostur, P. Talkner, J. Luczka, F. Marchesoni, and P. Hänggi, *Phys. Rev. E* **70**, 061105 (2004).
- [42] J. Spiechowicz, J. Łuczka, and P. Hänggi, *J. Stat. Mech.* (2013) P02044.
- [43] A. M. Fopossi Mbemmo, G. D. Kenmoe, and T. C. Kofane, *Eur. Phys. J. B* **89**, 211 (2016).
- [44] K. Lindenberg, J. M. Sancho, A. M. Lacasta, and I. M. Sokolov, *Phys. Rev. Lett.* **98**, 020602 (2007).
- [45] P. Jung, J. G. Kissner, and P. Hänggi, *Phys. Rev. Lett.* **76**, 3436 (1996).
- [46] G. Costantini and F. Marchesoni, *Europhys. Lett.* **48**, 491 (1999).
- [47] H. D. Vollmer and H. Risken, *Z. Phys. B* **34**, 313 (1979).
- [48] P. Jung, *Phys. Rep.* **234**, 175 (1993).
- [49] T. Chen, Ms. Sci., A theoretical and numerical study for the Fokker-Planck equation, Simon Fraser University, 1992.